Research Article

Active Site of Catalytic Ethene Epoxidation: Machine-Learning Global Pathway Sampling Rules Out the Metal Sites

Dongxiao Chen, Pei-Lin Kang, and Zhi-Pan Liu*

Read Online

ACCESS | Metrics & More | Article Recommendations | Supporting Information

ABSTRACT: Ethene epoxidation on Ag-based catalysts, an important heterogeneous catalytic reaction with large-scale global wide production, has generated continuous debate on the active site of epoxidation over the past 60 years. The controversy is not only on the roles of the phase transition from Ag metal to oxidation but also on the necessity of the minority crystal facets of the Ag metal, i.e., Ag(100). Herein, we identify, via a machine-learning reaction exploration, that ethene oxidation on the Ag metal surfaces has three low-energy pathways and the most important one, the dehydrogenation of oxometallacycle intermediate (OMC-DH), is entirely overlooked previously. By computing the free energy profile and performing microkinetics simulation, we show that irrespective of the reaction conditions the dehydrogenation path is always dominant for ethene oxidation on both Ag(100) and Ag(111) metal surfaces (>90%), which rationalizes the low selectivity to combustion products (CO_2 and H_2O) in low oxygen pressure experiments and rules out the chance of Ag metal phases being the active site of ethene epoxidation under industrial conditions (high O_2 pressures). The universal presence of the OMC-DH pathway and the general low selectivity on metal sites are then confirmed by evaluating this mechanism on different catalysts. Our results highlight the power of machine-learning-based reaction exploration for resolving the complex reaction network and also point the direction to reveal the true active site of Ag-based catalyst in ethene oxidation.

KEYWORDS: *ethene epoxidation, silver, mechanism, dehydrogenation, machine learning, DFT, microkinetics simulation*
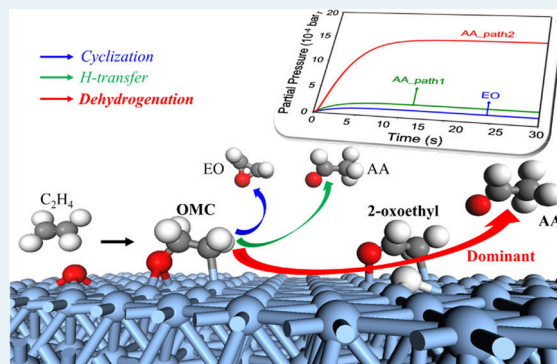
1. INTRODUCTION

Ethene epoxidation on Ag-based catalyst is the only viable path to produce ethene oxide (EO) in the industry with huge economic incentives (estimated global EO market to reach $64.1 billion by 2027).[1] The high selectivity to EO, a kinetically controlled product, has been constantly pursued,[2−6] which can be considered the result of competition between the desired epoxidation path ($C_2H_4 + 0.5O_2 \rightarrow C_2H_4O$, ΔH (298.15 K) = −105 kJ/mol) and the side-reaction path, i.e., the combustion of ethene to water and carbon dioxide ($C_2H_4 + 3O_2 \rightarrow 2CO_2 + 2H_2O$, ΔH (298.15 K) = −1327 kJ/mol).[7] To understand the reaction, silver metal has been popularly considered as a model system, which is shown to achieve about 50% selectivity with a low conversion (around 10%) only at the industrial conditions (e.g., 500 K and 20 bar with 5% of both ethene and oxygen).[8−11] The high sensitivity of selectivity to reaction conditions, especially O_2 pressure, has generated continuous debate on the active site of epoxidation over the past 60 years,[7,12] and the physical origin of the selectivity on Ag catalysts remains elusive.

To date, many mechanisms on ethene epoxidation have been proposed, such as molecular O_2 mechanism,[13] direct oxidation,[14,15] oxometallacycle (OMC) mechanism,[11,16,17] etc. Among them, the OMC mechanism is widely accepted with

experimental spectroscopy evidence on the OMC intermediate.[17] In this mechanism, as illustrated in Figure 1, ethene first combines with an adsorbed oxygen atom to form an OMC intermediate and then has two possible paths: the cyclization to EO and the 1,2-H-transfer to form acetaldehyde (AA), the precursor of combustion products as verified in the temperature-programmed reaction (TPR) spectrum.[18] It was thus believed that the competition between the cyclization and the H-transfer pathways controls EO selectivity.[19]

Based on this picture, early theoretical results using density functional theory (DFT) calculations appear to favor Ag metal as the active site for EO production[10,11,20] since both Ag(111) and Ag(100) achieve similar barriers for the two pathways. For example, on Ag(111), the Gibbs free energy barrier of cyclization is only 0.013 eV higher than that of H-transfer, suggesting ∼40% EO selectivity on Ag(111) at 400−500 K.[21] This is, however, not consistent with the surface science
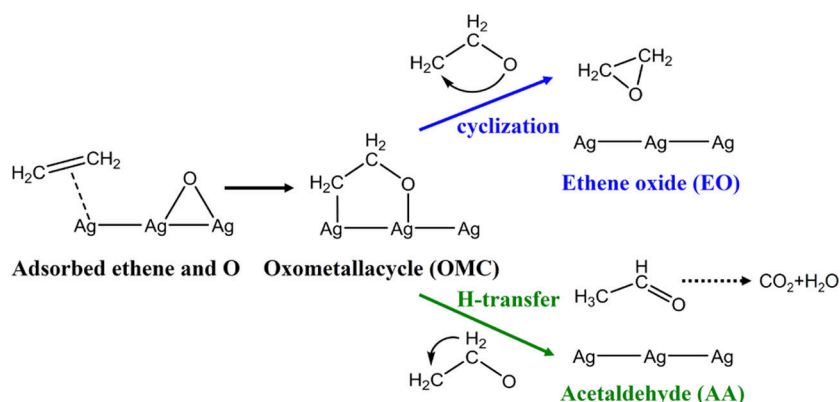
Figure 1. Proposed mechanism in literature studies for ethene epoxidation on silver catalysts via the OMC intermediate, in which EO is the desired product and CO_2 and H_2O are the combustion products.

experiment on the Ag single crystal surfaces. With the oxygen pressure (0.63 mbar) lower enough to avoid surface deep oxidation, the Wintterlin group had managed to detect only a trace production of EO on 1.1 cm^2 Ag(111) crystals with a selectivity of 2.0%, using quadrupole mass spectrometry (QMS) at 523 K.[22] Similar results were also found by Campbell's group on Ag(111), showing a low EO selectivity (<30%) under low oxygen pressure (<10 mbar).[23] With the recent advance in near-ambient pressure X-ray photoelectron spectroscopy (NAP-XPS), the Schlögl group[24] observed various oxygen species on Ag(111) at low O_2 pressures. The electrophilic O with the O 1s XPS signal at about 530 eV was suggested to be the O species for EO production as it appears along with the EO production.[25−28] These electrophilic O species were suggested to be from the impurity SO_4,[29,30] and also argued to be from O_3 species.[31] Due to the very low EO conversion and selectivity under low-pressure conditions, these understandings, such as on SO_4 impurities, should not be simply transferred to industrial EO production.

On the other hand, the structure of the Ag catalyst under industrial conditions was long known to be much more complex than the single-crystal Ag surfaces.[32−35] In particular, the structural characterization of Ag samples with high energy O species (atomic O, NO_2 reactants) has provided solid evidence on the presence of various surface oxides on Ag,[36−38] which are linked to the structures of the Ag catalyst at high O_2 pressures of industrial conditions, as also confirmed by the theoretical phase diagram.[33] These oxygen species form dynamically and were suspected to be the key reactive species for EO production.[37] To add more puzzles, a recent experiment seems to favor the minority Ag metal sites as the catalytic center. It was shown that at 510 K and the atmospheric pressure (with 10% of both ethene and oxygen), the performances of α-Al_2O_3-supported synthesized Ag nanowires, predominantly exposing the {100} facet, and commercial Ag nanoparticles with dominant {111} facets, exhibit 65 and 47% EO selectivity, respectively.[10] The minority {100} sites appear to be more active.

As pointed out by Pu et al. in a recent review,[7] "the Ag surface must become oxidized to generate the catalytic active oxygen sites responsible for ethene oxidation". There is a knowledge gap on the transition between Ag metal and oxides surfaces that leads to a poor understanding of the selectivity under different reaction conditions. As the first step to answer these questions, it is a must to revisit the generally accepted OMC mechanism on Ag metal surfaces for reconciling the

observations in surface science experiments and theoretical calculations.

With the help of machine-learning-based global potential energy surface (PES) exploration, here we are able to resolve the ethene oxidation reaction network on Ag surfaces in an automated way without the need for a priori knowledge. This leads to the discovery of a new low-energy pathway to the AA byproduct via the OMC dehydrogenation on Ag surfaces. Our microkinetics simulation based on the DFT free energy profile settles finally the long-standing puzzles on the low selectivity of epoxidation at low O_2 pressures, and thus, rules out the possible contribution of Ag metal surfaces to high EO selectivity. By extending our understanding to other catalysts, including Ag nanoparticles, Ag surface oxides, and Cu and Au surfaces, we prove the universal presence of a three-way mechanism for ethene epoxidation and the key role of the dehydrogenation pathway in decreasing the EO selectivity. The implication of searching for better epoxidation catalysts is discussed after the catalyst electronic structure analyses.

2. METHODS

2.1. Machine-Learning Atomic Simulation. In this work, we have generated the first quaternary Ag−C−H−O global neural network potential for the structure and pathway search using the stochastic surface waling (SSW) method based on the global neutral network (G-NN) potential. The details of the method are reported previously and also in the Supporting Information, Section 1.[39−42] The data set for G-NN training is obtained iteratively by the SSW global potential energy surface (PES) searching, which has 47 147 structures in total, containing the bulk and surfaces of Ag and AgO_x, as well as different C−H−O molecules on Ag and AgO_x surfaces, as detailed in Table S1. The G-NN has a three-hidden layer (305-80-50-50-1 net) feedforward NN architecture for each element, which reaches 124 524 parameters in total. The final root mean square (RMS) errors for the energy and force were 2.73 meV/atom and 0.08 eV/Å, respectively, which is accurate enough for the exploration of PES and the identification of reaction pathway. Our benchmark between G-NN and DFT results for the calculated energies of some reaction pairs and reaction barriers is shown in Tables S2 and S3.

2.2. Automated SSW-RS Method for Pathway Search. To explore all of the likely pathways for ethene epoxidation, we have utilized SSW-based reaction sampling (SSW-RS) to build up the reaction network. While the method was utilized
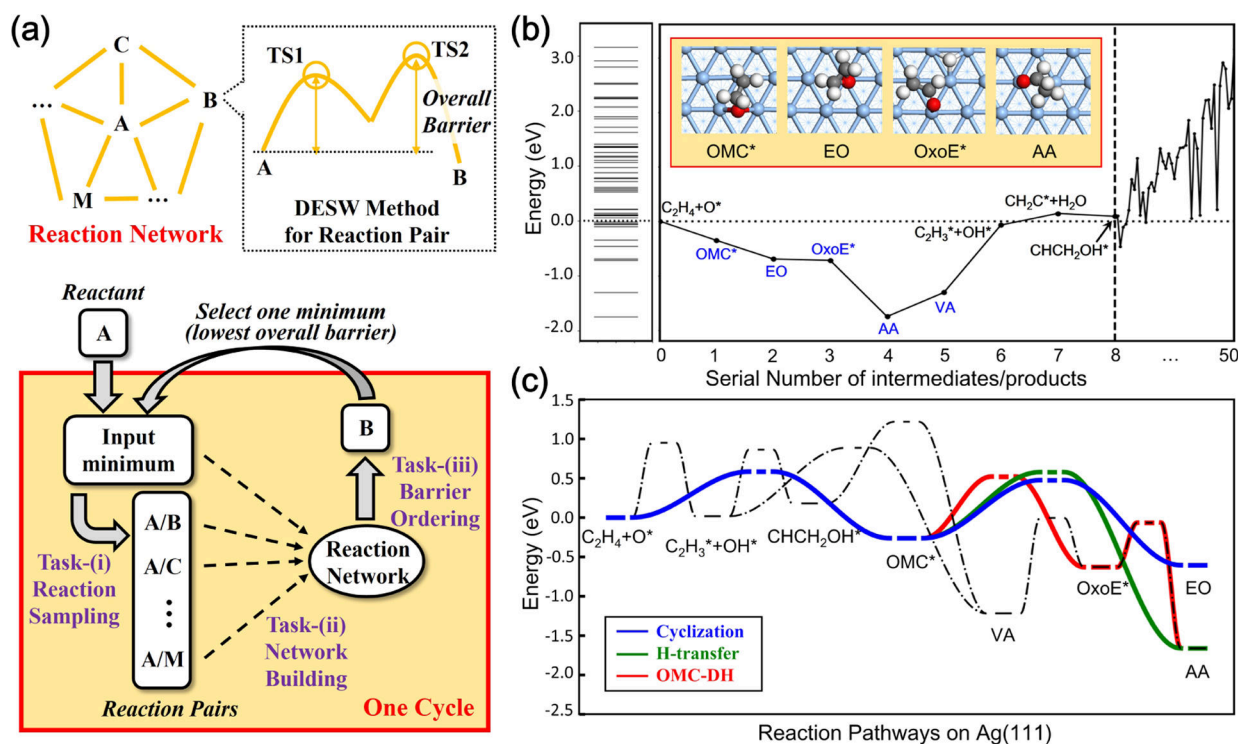
Figure 2. (a) SSW-RS method to resolve the catalytic reaction network in an automated way. (b) SSW-RS results for ethene epoxidation. The simulation starts from ethene in the gas phase and an adsorbed O on Ag(111). The left bar code denotes the energy spectrum of the low-energy minima along different oxidation pathways, and the right figure resolves these minima in the order of their overall formation barriers from low to high, in which the minima with the barrier smaller than 1 eV are indicated by name. Abbreviations. OMC: oxometallacycle; EO: ethene oxide; OxoE: 2-oxoethyl; AA: acetaldehyde; VA: vinyl alcohol. (c) The top 5 pathways with the lowest overall barriers in ethene oxidation on Ag(111), in which the three pathways bifurcating at OMC are highlighted in color.

previously in combination with DFT calculations for crystal phase transition,[43,44] the advent of G-NN potential allows the SSW-RS simulation to perform much more efficiently,[45] and thus, is applied to large-size systems, such as molecules on surfaces.

As shown in Figure 2a, we can consider a reaction network as a graph with nodes and edges, each node and edge representing a distinct minimum and a pathway between minima, respectively. SSW-RS can resolve a reaction network by iteratively performing three consecutive tasks: (i) exploring the likely pathways of a selected minimum on PES that is the reactant initially (e.g., ethene and an adsorbed atomic O on the Ag surface in this work) and will be replaced by other intermediates in subsequent cycles; (ii) identifying all of the transition states (TSs) for the pathways collected in task (i) and compare the overall barriers for each minimum starting from the initial reactant; and (iii) ordering the overall barrier, an intermediate with the lowest overall barrier and not being sampled in task (i) is preferentially selected as the new minimum and then the next cycle starts by returning to task (i).

In the above tasks, task (i) yields a library of reaction pairs (initial state/final state, IS/FS) linking from the sampled minimum to the minimum nearby. The structural similarity between different states (molecules on surfaces) is judged based on the bond matrix of adsorbates and the Euclidean distance between structures. Task (ii) identifies the low-energy pathway and locates the TS for each reaction pair using the double-ended surface walking (DESW) method.[46] This is achieved by driving two images from IS and FS toward each other via the consecutive addition of bias Gaussian potential.

After the path is connected, the constrained Broyden dimer (CBD) method[47] starting from the maximum energy point along the path is then utilized to locate the TSs, which are further confirmed by vibrational frequency calculations and the extrapolation optimization to the correct IS and FS.

2.3. DFT Calculations. All DFT calculations were performed using the plane-wave VASP package,[48] in which the electron−ion interaction was represented by the projector-augmented wave (PAW) pseudopotential,[49] and the exchange functional was evaluated with the GGA-PBE.[50] The energy cutoff was set as 450 eV, and the convergence criterion of energy was set to be 10^{-6} eV, while that of the force was 0.02 eV/Å for stable structures and 0.05 eV/Å for TSs. As for metal surfaces, a four-layer slab model with $p(4 \times 4)$ supercell was utilized, where the bottom two layers were kept fixed in the bulk truncated positions. The Monkhorst−Pack k-mesh was 30 times the reciprocal lattice vectors (1/30 Å^{-1}, i.e., (3 × 3 × 1) mesh for the $p(4 \times 4)$ Ag surface). It should be mentioned that while G-NN calculations are utilized initially for pathway searching, all reaction data reported in this work without explicitly mentioning are from DFT calculations to compare accurately our theoretical predictions with experiments.

To construct the free energy profile under the reaction conditions and perform microkinetics, we have considered the free energy corrections for gas-phase molecules and vibrational zero-point energy (ZPE) for all surface states. The free energy corrections of the gas-phase molecules are obtained from standard thermodynamics equations, which are −1.06, −0.99, −1.31, and −1.40 eV for 1 bar of ethene and oxygen, and 0.05 bar of EO and AA at 500 K, respectively (the typical reaction conditions with 50% selectivity and 10% conversion).[51] The
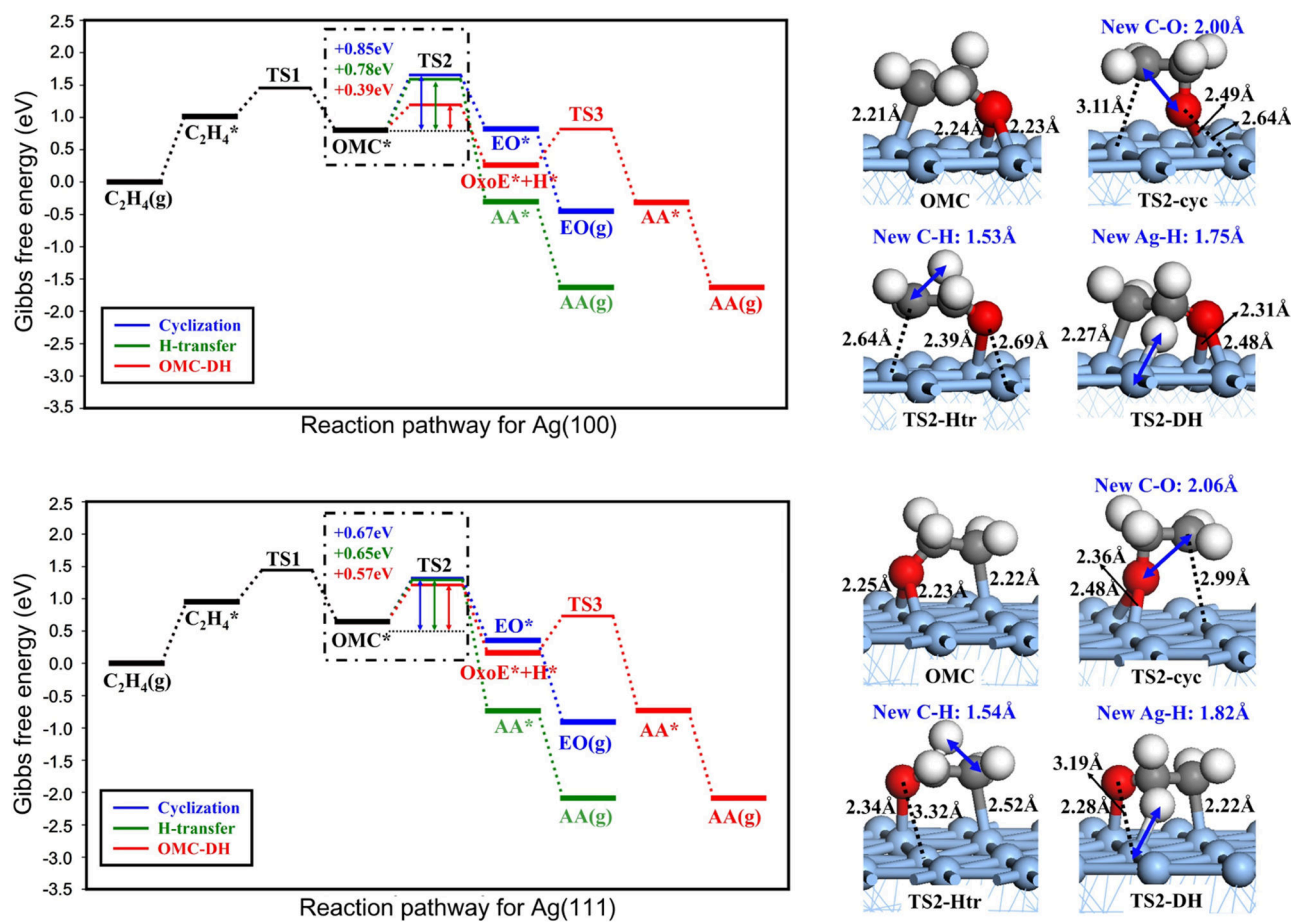
Figure 3. Gibbs free energy profiles for ethene oxidation on pristine Ag(100) and Ag(111) under industrial conditions (500 K and 1, 0.05, 0.05 bar of ethene, EO, and AA, respectively). The reaction snapshots of the OMC intermediate and three TS2s are also shown with key bond lengths labeled. Color scheme of atoms: Ag, blue; C, gray; H, white; and O, red.

Gibbs free energy of the surface state is set to be the ZPE-corrected DFT total energy since the entropy and thermal contribution are negligibly small.[52]

3. RESULTS

3.1. SSW-RS Reaction Sampling for Ethene Oxidation.
With machine-learning-based reaction sampling, we are able to build the reaction network of ethene oxidation on Ag surfaces in an automated way, which not only vastly reduces the manual efforts to explore the likely mechanism but also helps to identify the unexpected new reaction channels. Our SSW-RS simulation starts from ethene and an atomic adsorbed oxygen (O*), the reactant, on the silver surface ($p(4 \times 4)$ slab). In total, more than 26 cycles with 20 000 SSW steps per cycle are carried out, which leads to the identification of 56 and 50 low-energy intermediates/products, and 7600 and 7967 reaction pairs connecting them for Ag(100) and Ag(111), respectively. Finally, the TSs for all these pairs are located, from which the lowest energy pathways are determined.

We now consider Ag(111) as an example to illustrate the SSW-RS results (results of Ag(100) are described in the Supporting Information, Section 2 and Figures S1 and S2). The energies in this section are based on G-NN calculations directly from all SSW-RS simulations.

Figure 2b shows the energy spectrum of all of the sampled 50 products (left) and the name of them sorted by their overall formation barrier from low to high (right). While there are 8

structures with relatively low formation barriers (<1 eV), only the top five structures (marked blue in the figure) are both thermodynamically stable and kinetically facile to reach (exothermic in reaction and <0.78 eV in the overall formation barrier). Importantly, these five products contain the known intermediates in the experiment, including the OMC intermediate (ranked 1st, exothermic by 0.35 eV with a barrier of 0.58 eV), EO and AA products (ranked 2nd and 4th, exothermic by 0.70 and 1.75 eV with barriers of 0.74 and 0.78 eV, respectively). There are also unexpected products, such as vinyl alcohol (VA) and 2-oxoethyl (OxoE), which can be regarded as the well-known fast keto−enol tautomer of AA and the dehydrogenated product of OMC, respectively. The most stable configuration of OxoE is also shown in Figure 2b, where its terminal C and O bond with the surface, and the dissociated H is at the nearby threefold hollow site.

As for the products with low stability, there are the intermediates from direct C−H bond breaking of ethene (vinyl and hydroxyl, ranked 6th), adsorbed carbene species (CCH$_2$* + H$_2$O and CHCH$_2$OH*, ranked 7th and 8th, respectively), and also the C1 species like formaldehyde. These products generally also need to overcome the high barrier to form, and thus, unlikely to form in reality. The appearance of these high-energy products from SSW-RS implies the completeness of the pathway sampling for important low barrier reactions.

Now, we can focus on the lowest energy pathways, as plotted in the energy profile (Figure 2c). We found that the ethene to EO pathway identified from SSW-RS is consistent with the previous literature studies, that is, only the cyclization pathway has a low barrier and should thus be responsible for EO production (blue line). On the other hand, the ethene to AA pathway is rather unexpected, and a number of low-energy pathways emerged from SSW-RS (the overall barriers are smaller than 1 eV). We found that in addition to the cyclization pathway, two other pathways (green and red lines) are also via the OMC intermediate but tend to produce AA. Interestingly, the traditionally regarded H-transfer process via OMC to form AA (green line) is in fact competing with a more favored new pathway (red line) with a barrier difference of only 0.06 eV. This new pathway, denoted as OMC-DH, is a two-step reaction via the OMC dehydrogenation to form the OxoE intermediate, and then hydrogenation to form AA or VA (see Figure 2c). It should be mentioned that the OMC-DH pathway is also present on Ag(100), which is 0.35 eV lower than the H-transfer pathway (see Figure S2 and Table S3).

For other less favored pathways, they do not bypass the OMC intermediate but undergo the direct dehydrogenation of ethene to form the adsorbed vinyl group. These pathways are kinetically avoided because the ethene dehydrogenation barrier is 0.37 eV higher than that of the OMC formation. Our results are consistent with the previous theoretical work on Ag surfaces,[53] which suggests that the OMC intermediate is the kinetically selected product.

To summarize, SSW-RS shows that ethene epoxidation on Ag surfaces follows a three-way mechanism via the same OMC intermediate, including the OMC cyclization to EO, the H-transfer to AA, and the new OMC-DH pathway. To further confirm these G-NN simulation findings, we further conducted DFT calculations to validate the low-energy pathways, which gave essentially the same conclusion. In Section 3.2 and 3.3, we will analyze in detail the kinetics of the low-energy pathways on two Ag surfaces based on DFT results.

3.2. DFT Pathways on Ag(100) and Ag(111). For the three lowest energy pathways, we first determined the Gibbs free energy profiles based on DFT energetics, as shown in Figure 3. It can be seen that the OMC-DH pathway (red line) is always the lowest barrier pathway on both surfaces.

The free energy profile on Ag(100) is elaborated as follows. The adsorption of ethene on Ag is highly endothermic by 1.02 eV due to the weak adsorption of ethene (−0.04 eV) and the large entropy loss at 500 K reaction conditions. The ethene can react with the O atom with a barrier of 0.42 eV (TS1 in Figure 3) to form an OMC intermediate. The adsorbed OMC prefers the bridge-adsorbed configuration at its O end, which is slightly more stable (0.07 eV) than the configuration of O at the hollow site. The OMC then has three possible routes to produce EO, AA, and OxoE (TS2-cyc, TS2-Htr, TS2-DH), where OMC adopts different precursor geometries (structures in Figure 3). The barriers are 0.85 eV for cyclization to EO, 0.78 eV for H-transfer to AA, and only 0.39 eV for dehydrogenation to OxoE and an adsorbed H. For the cyclization step, the oxygen first shifts from the bridge site to the hollow site and then links with the terminal C in achieving the TS (TS2-cyc), where the C−O distance is 2.00 Å. Both the H-transfer and the DH pathway first require the breaking of the α-C−H bond of OMC. After passing through the α-C−H breaking TSs, a new C−H or a Ag−H bond with a distance of 1.53 or 1.75 Å at the TS evolve to form the AA or OxoE,

respectively. We note that the β-C starts to leave the Ag surface at the TS2-cyc and TS2-Htr, which have a Ag−C distance of 0.90 and are 0.43 Å longer than that in the initial OMC.

As for the atomic H produced in the OMC-DH pathway, it can react with the terminal C of OxoE to form AA via TS3, in Figure 3 with a barrier of 0.55 eV. Alternatively, the H may also react with the terminal O of OxoE to form VA, or diffuse away to react with the other surface O (O* + H* → OH*) considering that H diffusion on Ag has a low barrier. For these possible pathways, the VA formation from OxoE has a comparable barrier with that of the hydrogenation to AA, while the OH* formation is the least likely pathway (see Figure S3). Considering that the formation of AA, VA, and OH* are all exothermic (see Figures 3 and S3), once the dehydrogenation occurs the full oxidation would be inevitable, indicating the key role of the dehydrogenation reaction to decrease the epoxidation selectivity. Finally, the EO and AA products can desorb readily from the surface since they adsorb only weakly on Ag (adsorption energy of 0.04 eV for EO and 0.07 eV for AA).

While the mechanism of ethene oxidation on Ag(111) is the same as that on Ag(100), the three pathways have quite different geometries and energetics on the two surfaces (Figure 3). The differences between (111) and (100) are highlighted as follows.

(i) Fewer Ag atoms take part in the TS. There are only three Ag atoms involved in the TSs on Ag(111), but four Ag atoms on Ag(100). As a result, for all TS2 on Ag(100), the O atom of OMC remains at the bridge site, but the O atom has to shift to the atop site for the TS2-Htr and TS2-DH on Ag(111).

(ii) The poorer O atom adsorption. Compared with Ag(100), the atomic O has a lower stability on Ag(111). As a result, the reaction from ethene and adsorbed O to the final product EO(g) and AA(g) are more exothermic on Ag(111) (by 0.46 eV). The relative stability of OMC on Ag(111) is also higher: +0.65 on Ag(111) and +0.81 on Ag(100).

(iii) The narrower reaction barrier difference for three pathways. The relative stability of TS2 follows the order of TS2-cyc > TS2-Htr > TS2-DH on Ag(111), the same as that in Ag(100), but the barrier difference between them is much reduced on Ag(111). For example, the energy difference between the TS2-Htr and TS2-DH is 0.39 eV on Ag(100) but only 0.08 eV on Ag(111). This suggests that the OMC-DH pathway on Ag(111) is not as dominant as that on Ag(100).

It should be noted that the barriers of the three OMC transformation pathways can be rather close, e.g., <0.1 eV on Ag(111), which is within the typical error bar of DFT calculations (also see Table S4). We thus have also examined the key results using different functionals (PW91, RPBE) and with van der Waals (vdW) corrections (Table S4). It shows that the inclusion of the vdW interaction will not affect the order of barriers and thus the selectivity. This is also true for the coverage of O atoms up to 1/4 ML on Ag(111) (see Table S5). By comparing with known experimental results on Ag(111),[22,23] we confirm that DFT results with the PBE functional are reliable for predicting the selectivity.

It is of interest to compare our DFT results with the previous literature studies, where the PBE or PW91 functional was mostly used to investigate the cyclization and the H-
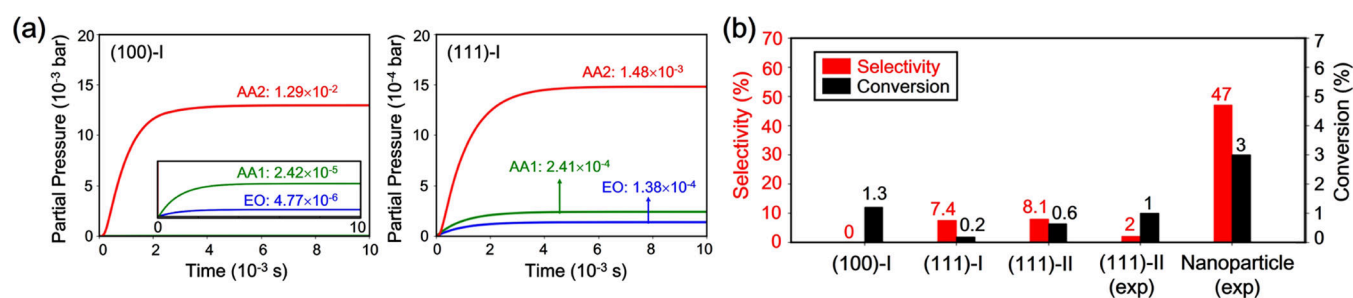
Figure 4. Microkinetics simulation results under two typical experimental conditions. Condition I: typical industrial conditions, i.e., 500 K and $p(C_2H_4) = p(O_2) = 1$ bar; condition II: the low oxygen pressure conditions often used in surface science experiments, i.e., 523 K, $p(C_2H_4) = 0.63$ mbar, and $p(O_2) = 0.36$ mbar. (a) The partial pressures of EO, AA1 (AA produced via the H-transfer pathway), and AA2 (AA produced by the OMC-DH pathway) species versus time on pristine Ag(100) and Ag(111) under condition I. (b) The ethene conversion and EO selectivity from our simulation and from the previous experiment (exp) at the two conditions. Experimental results of Ag(111) at condition II are from ref 22 and those of supported Ag nanoparticles at condition I are from ref 10.

transfer pathways (also see in Table S6). For Ag(111), by combining the frequency calculations on a Ag$_{15}$ cluster and the geometry optimization on the periodic Ag(111) model, Linic and Barteau[21] obtained the Gibbs free energy barrier difference of 0.013 eV (0.3 kcal/mol) between the two pathways, where the H-transfer pathway is slightly preferred. This is consistent with the 0.02 eV obtained in this work. Other DFT calculations, despite different computational models and settings, generally predict not more than 0.06 eV difference between the cyclization and the H-transfer pathway on Ag(111).[53] For Ag(100), using a $p(2 \times 2)$ supercell of Ag(100), Özbek et al.[53] obtained ZPE-corrected EO and AA formation barriers of 0.75 and 0.68 eV (72 and 66 kJ/mol), which are slightly lower than the 0.85 and 0.78 eV obtained in this work. The ∼0.1 eV differences for EO and AA formation barriers on Ag(100) are also reported by several groups.[10,11] It should be emphasized that the lower barrier of the OMC-DH pathway, especially on Ag(100) identified in this work, invalidate the previous kinetics models for estimating selectivity using only the cyclization and the H-transfer pathways.[11,19,54] The barrier difference of the two pathways is no longer important to determine the selectivity, as clearly supported in Section 3.3.

3.3. Microkinetics Simulation. To examine EO selectivity, we then conducted the microkinetics simulation for ethene oxidation with all of the reaction data from DFT. A continuous-stirred tank model is used in simulation, and the kinetic equations are iteratively solved until the contents of the species are in equilibrium.[55] More details on our microkinetics simulation setup and the comparison with the previous work[11] are shown in the Supporting Information, Section 4. All of the reaction data for microkinetics simulation are shown in Table S7. To examine the influence of O$_2$ pressure, we consider two conditions utilized in the experiment: (i) condition I—at typical industrial conditions with C$_2$H$_4$ and O$_2$ being both at 1 bar, 500 K;[54] (ii) condition II—at low oxygen pressure conditions with 0.63 mbar of ethene and 0.36 mbar of oxygen at 523 K.[22]

Our simulation results on the production of EO and AA with time are shown in Figure 4a, and the equilibrium volumes for all of the species are given in Table S8 (our results with the PBE-D3-corrected energies are also shown in Table S9, which can yield higher rates but remain at low EO selectivity). To better distinguish the source of AA, we use AA1 and AA2 to denote the AA generated from the H-transfer and OMC-DH pathways, respectively. In Figure 4a, we show that for

condition I, after about 0.005 s, the system reaches a steady state. In the steady state, AA2 is the dominant product, being about 10 times more than AA1 and EO on Ag(111) and 10^4 times more on Ag(100). The production of AA1 and EO are low and have a similar order of magnitude. Overall, as shown in Figure 4b, the selectivity to EO is zero and 7.4% for Ag(100) and Ag(111), respectively. When switching to condition II, we found that the low EO selectivity does not change much: the selectivity on Ag(111) only slightly increases from 7.4 to 8.1% when the ethene and oxygen pressures drop below 1 mbar at 523 K. These results suggest that the OMC-DH pathway is always the dominant pathway on both the Ag surfaces, independent of the O$_2$ pressure.

Now, we are in a position to compare our kinetics results with the experimental data (note that the previous theoretical work[11] overlooked the OMC-DH pathway and we have discussed this issue in Figure S4). As shown in Figure 4b, the Wintterlin group found that under condition II, the EO selectivity is 2% at 1% conversion on Ag(111).[22] Although the EO production under condition II might be from impurities,[29] our results for O/Ag surfaces also predict low conversion and low selectivity. It might be noted that the defective sites (steps, edges) could also contribute to the overall activity,[11] which is not considered here. For the experiments at high oxygen pressures, the maximum selectivity can be more than 47% with ethene conversion of 3%,[10] which is obviously higher than our theoretical results. This indicates that the metallic Ag is not the catalytic site under high oxygen pressures.

4. DISCUSSION

4.1. EO Selectivity in the Context of Three-Way Mechanism. To examine the generality of the three-way mechanism for ethene epoxidation, we go beyond the Ag crystal surfaces to examine ethene oxidation on a series of other catalysts, as shown in Figure 5a. These catalysts include three types: (i) a partially oxidized Ag surface with a $p(4 \times 4)$ pattern observed in the experiment after the pre-oxidization of Ag(111),[56,57] and is denoted as Ag-surf-oxide. The surface O is four-coordinated with the surface Ag atoms in the surface oxide, which is similar to that in Ag(100). (ii) A Ag nanoparticle Ag$_{55}$ with the exposure of (111) facet. (iii) The (111) surface of Cu and Au crystals. The Ag-surf-oxide has been extensively studied previously and shown to exhibit no EO selectivity in the experiment;[58] Ag$_{55}$ is an icosahedral cluster[59−61] and is regarded to be the model for silver nanoparticles in the supported industrial catalyst (Ag/Al$_2$O$_3$);
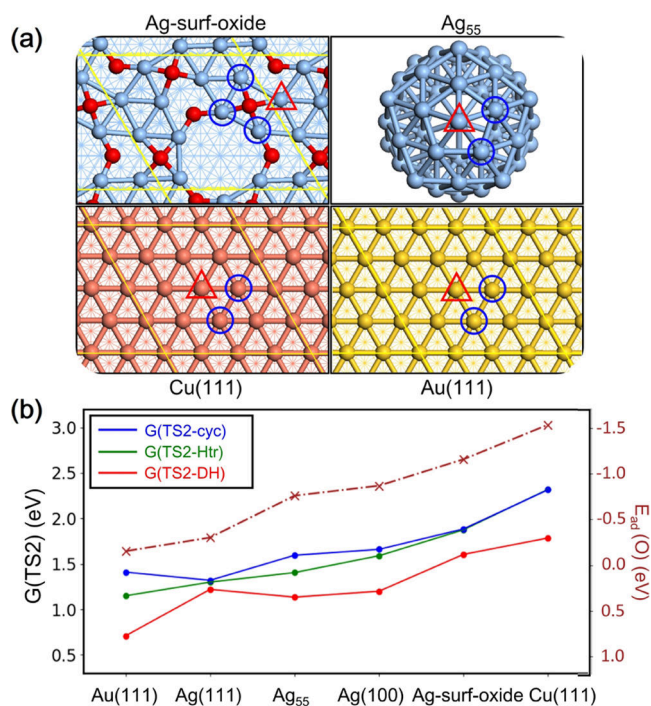
Figure 5. (a) Atomic structure of the partially oxidized Ag surface (Ag-surf-oxide), silver nanoparticle Ag_{55}, and Cu(111) and Au(111). The metal atoms in the reaction are highlighted by blue circles and red triangles (the ethene adsorption site). (b) DFT-calculated Gibbs free energies of three TS2s on different catalysts. The free energy zero is set as that of the initial reactant (ethene in the gas phase and the adsorbed O atom). The O adsorption energies ($E_{ad}(O)$, with respect to half of the gas phase O_2) on these catalysts are also plotted.

and Cu and Au are group IB noble metals, same as Ag, and also poor catalysts with low activity for ethene oxidation in the presence of O_2.[62,63]

Since the selectivity is determined by the relative rate of the three pathways initiated from OMC, here, we compare directly the calculated Gibbs free energies of TS2, G(TS2), for three pathways (G(TS2-cyc), G(TS2-Htr), and G(TS2-DH)) with respect to the reactant (adsorbed O on the surface and an ethene in the gas phase). These catalysts have similar reaction routes as those on Ag surfaces, and the determined ethene adsorption and O coordination sites on them are labeled in Figure 5a. For the Ag-surf-oxide and Ag_{55} nanoparticle where multiple reaction sites are available, we found that the most stable TS is achieved at the edge of the triangle Ag_6 and the low coordinated apex Ag, respectively. Our results for G(TS2) data are summarized in Figure 5b, and the detailed information is shown in Table S10 and Figures S5−S8.

Importantly, we found that G(TS2-DH) (red line) is always the lowest among the three likely pathways for all of the catalysts examined, indicating the universal presence and the importance of the OMC-DH pathway. In general, the trends of G(TS2-cyc) and G(TS2-Htr) are close to each other (green and blue lines) but the trend of G(TS2-DH) (red line) is different, showing a plateau on the three Ag metal catalysts (differs by not more than 0.10 eV).

Now, we focus on four different Ag systems (three Ag metals and one Ag surface oxide). We found that the small particle Ag_{55} will increase G(TS2-cyc) and G(TS2-Htr) by 0.28 and 0.11 eV, respectively, compared to those in Ag(111), but affects slightly the G(TS2-DH). This indicates that the presence of low-coordinated Ag (apex Ag has only 6-coordination) will reduce the selectivity. For the Ag-surf-oxide, all G(TS2) are much larger than those on the Ag metal surfaces, indicating the relative inertness of the positively charged Ag that reduces the activity. For selectivity, the energy difference (0.28 eV) of G(TS2-cyc) and G(TS2-DH) on the Ag-surf-oxide is smaller than that (0.46 eV) in Ag(100) but larger than that in Ag(111); thus, the selectivity is not obviously improved over the Ag metal.

To understand the trend of G(TS2), we have compared the adsorption energies of O atom on these surfaces, as also shown in Figure 5b. While calculating the O atom adsorption energy ($E_{ad}(O)$), we consider the O atom that will react with ethene during epoxidation, i.e., the adsorbed O atom on the metal surface and the fourfold surface O atom on the Ag-surf-oxide. From Figure 5b, it is clear that the adsorption energy of the O atom has a strong correlation with G(TS2-cyc) and G(TS2-Htr): the stronger the O adsorption, the higher the G(TS2-cyc) and G(TS2-Htr). This finding may not be surprising since both the cyclization and the H-transfer reactions are required to break the O-surface bonds to form the EO and AA molecules at the final state. As evident in the TS structures in Figure 3, the O atom moves appreciably away from the surface in achieving the TSs of the cyclization and the H-transfer reaction, where the O−Ag bonding is much weakened.

On the other hand, the trend of O atom adsorption energy does not exactly coincide with the trend of G(TS2-DH), mainly because of the plateau of G(TS2-DH) on the three Ag metal surfaces. It implies that, in addition to the O adsorption energy, other factors also play important roles in the stability of the TS2-DH. Indeed, the O−Ag bond distances for the dehydrogenation reaction also increase from the initial OMC to the TS (see Figure 3) but less significant compared to the other two TSs. The major change occurs at the C−H bond breaking, which leads to the formation of the new H−Ag bond and sp^2-hybridized α-C. It is, therefore, important to consider

Table 1. Atomic Bader Charge Analyses on the TS of Dehydrogenation (TS2-DH, see Figure 2)[a]

catalysts	α-C(TS)	β-C(TS)	H(TS)	**M(TS)**	O(TS)	**Δα-C**	**Δβ-C**	**ΔH**	**ΔM**	**ΔO**	**G(TS2-DH) (eV)**
Au(111)	+0.70	−0.30	−0.01	**+0.05**	−1.04	**+0.83**	−0.17	−0.08	−0.11	−0.30	**0.71**
Ag(111)	+0.68	−0.30	−0.10	**+0.09**	−1.10	**+0.81**	−0.17	−0.17	−0.09	−0.25	**1.22**
Ag_{55}	+0.67	−0.25	−0.09	**+0.11**	−1.10	**+0.80**	−0.12	−0.16	−0.10	−0.24	**1.14**
Ag(100)	+0.65	−0.25	−0.10	**+0.11**	−1.10	**+0.78**	−0.12	−0.17	−0.08	−0.11	**1.20**
Ag-surf-oxide	**+0.41**	−0.25	−0.01	**+0.24**	−1.05	**+0.54**	−0.12	−0.08	−0.12	−0.15	**1.60**
Cu(111)	+0.59	−0.33	−0.14	**+0.13**	−1.09	**+0.72**	−0.20	−0.21	−0.12	−0.16	**1.79**

[a]The listed data include the atomic charge on the dissociating H (H), α-C, β-C, O, and the metals in reaction (M, on average) and the charge differences (Δ) of these atoms at the TS2-DH with respect to the initial state (gas-phase ethene and adsorbed atomic O). G(TS2-DH) is also listed for comparison.

the evolution of α-C bonding. To this end, we have performed Bader atomic charge analysis[64] for the TS2-DH and the reactant as shown in Table 1, which lists the net charge for the dissociating H, α-C, β-C, O, and the metals coordinated with the TS complex (M, labeled in Figure 5a, on average) at the TS2-DH and the charge differences from the reactant to the TS2-DH on these atoms.

Table 1 shows that the major feature of the TS2-DH is the accumulation of positive charges on the α-C$^{\delta+}$ during dehydrogenation ($\Delta\alpha$-C in the range of +0.54 to +0.83, in bold), which is caused largely by the internal polarization of the $[C_2H_4O]$ entity. The electron on α-C shifts to all neighboring atoms, including the O, the β-C, the dissociating H, and the metals. Comparing different catalysts, we found that the extent of charge accumulation on α-C is the lowest in Ag-surf-oxide and is similar in other Ag metal systems. We can, therefore, attribute the low stability of TS2-DH in Ag-surf-oxide to the poor ability to form α-C$^{\delta+}$. Since Ag atoms on the surface of Ag-surf-oxide are already positively charged (+0.36, see Table 1), the through-space electrostatic repulsion between α-C$^{\delta+}$ and the cationic surface Ag atoms destabilizes TS2-DH, leading to a higher G(TS2-DH) than other three metallic Ag catalysts. The trend of G(TS2-DH) can thus be qualitatively understood by taking into account both the O atom adsorption and the surface cationic state.

While the previous theoretical studies suggested the adsorption strength of O (like OCH$_3$ group) affects selectivity,[65] i.e., the weak O-surface bonding is beneficial to the selective oxidation of ethene,[66,67] our results indicate that these statements are not complete because of neglecting the dehydrogenation pathways. From Figure 5, the weak Ag−O bonding may benefit the activity but certainly not the key factor to selectivity. Instead, we propose that the cationic state of the metal could be the key to depress the dehydrogenation channel and thus increase the selectivity. Nevertheless, for the Ag-surf-oxide with cationic Ag, the barrier of the dehydrogenation pathway increases, and the other two pathways, the cyclization and the H-transfer, also have increased barriers due to the surface O with four-coordination with two Ag$_6$ patterns (see Figure 5a) has large adsorption energy. This implies that other more reactive O (less adsorption energy) on the cationic AgO$_x$ surfaces might be the true active sites for ethene epoxidation under industrial conditions. We expect that a good catalyst for epoxidation should not only possess the weak O-surface bonding that benefits EO formation but also contain the cationic surface atoms that inhibit the dehydrogenation reaction channel.

4.2. Active O Species for Epoxidation Under Industrial Conditions. To date, the active O species for epoxidation remains elusive under industrial conditions. The available key experimental data, such as isotope labeling[68] and in situ XPS experiments,[24] were all collected at the surface science conditions (low O$_2$ pressure), which identified different oxygen species, and only the electrophilic oxygen was found to be active for EO formation. While the nature of the electrophilic oxygen is still in debate,[24] recent experimental work suggested that these active O comes from SO$_4$ impurities.[29,30] However, since the selectivity under low pressures is typically below 10%, being far less selective than that at high pressures,[23] it is questionable to attribute the massive EO production at high pressures to the SO$_4$ contamination. In particular, the electrolytic Ag samples (triple refined) were long known to be excellent EO catalysts that are

99.999% pure,[69] and the input gas for epoxidation needs to be purified to remove sulfur contamination in industry.[70] Further studies are required to reveal the active O species at high pressures.

Our results with the new OMC-DH pathway now establish the complete reaction mechanism of epoxidation, which appears to be consistent with all known experimental findings. The general presence of the low-energy OMC-DH pathway over different metals (Cu, Ag, Au) and different Ag sites (nanoparticles and surface oxides) points to the future direction to search for the true active site for Ag-based industrial catalyst. By excluding the metallic Ag sites, the deep-oxidized Ag sites with subsurface O and those related to the other elements (such as SO$_4$ additive) become the most likely choices. With the methodology for automated pathway sampling and powerful G-NN potential generation, we believe that the active site in real catalytic systems for epoxidation can be identified in the near future.

5. CONCLUSIONS

With the advent of G-NN potential, this work revisits the reaction network of ethene oxidation on silver surfaces using automated global reaction sampling. A new dehydrogenation pathway accounting for the combustion of ethene is discovered on Ag surfaces, which has a lower barrier than the other two traditionally regarded pathways, the cyclization and the H-transfer pathways. From first-principles free-energy profiles of the three-way mechanism and microkinetics simulation, we now rule out from theory the possibility of Ag metal as the active site for the selective ethene epoxidation under industrial conditions.

By evaluating the three-way mechanism on a series of catalysts, including Ag nanoparticles, partially oxidized Ag, and Cu and Au surfaces, we confirm the universal presence and the general preference of the dehydrogenation pathway in ethene oxidation. Even for the partially oxidized Ag surface, EO selectivity remains poor since its surface O atoms are too strongly bonded, but it does shows promise for the inhibition of the dehydrogenation pathway due to the formation of cationic surface Ag sites.

■ ASSOCIATED CONTENT

ⓢ Supporting Information

The Supporting Information is available free of charge at https://pubs.acs.org/doi/10.1021/acscatal.1c02029.

> SSW-NN methodology and G-NN potential construction; reaction sampling and pathways on Ag(100) surface; more DFT results on pathways; microkinetics simulation; results on the Ag-surf-oxide, Ag55, Cu(111), and Au(111); XYZ coordinates for important structures along the OMC-DH pathway (PDF)

■ AUTHOR INFORMATION

Corresponding Author

Zhi-Pan Liu − *Collaborative Innovation Center of Chemistry for Energy Material, Shanghai Key Laboratory of Molecular Catalysis and Innovative Materials, Key Laboratory of Computational Physical Science, Department of Chemistry, Fudan University, Shanghai 200433, China;* ⓞ orcid.org/0000-0002-2906-5217; Email: zpliu@fudan.edu.cn

Authors

Dongxiao Chen − *Collaborative Innovation Center of Chemistry for Energy Material, Shanghai Key Laboratory of Molecular Catalysis and Innovative Materials, Key Laboratory of Computational Physical Science, Department of Chemistry, Fudan University, Shanghai 200433, China*

Pei-Lin Kang − *Collaborative Innovation Center of Chemistry for Energy Material, Shanghai Key Laboratory of Molecular Catalysis and Innovative Materials, Key Laboratory of Computational Physical Science, Department of Chemistry, Fudan University, Shanghai 200433, China*

Complete contact information is available at:
https://pubs.acs.org/10.1021/acscatal.1c02029

Notes

The authors declare no competing financial interest.

■ REFERENCES

(1) *Global Ethylene Oxide (EO) Industry*; Global Industry Analysts Inc., 2021; p 186.

(2) Diao, W.; DiGiulio, C. D.; Schaal, M. T.; Ma, S.; Monnier, J. R. An Investigation on the Role of Re as a Promoter in Ag-Cs-Re/Alpha-Al$_2$O$_3$ High-Selectivity, Ethylene Epoxidation Catalysts. *J. Catal.* **2015**, *322*, 14−23.

(3) Rocha, T. C. R.; Haevecker, M.; Knop-Gericke, A.; Schloegl, R. Promoters in Heterogeneous Catalysis: The Role of Cl on Ethylene Epoxidation over Ag. *J. Catal.* **2014**, *312*, 12−16.

(4) Greiner, M. T.; Cao, J.; Jones, T. E.; Beeg, S.; Skorupska, K.; Carbonio, E. A.; Sezen, H.; Amati, M.; Gregoratti, L.; Willinger, M.-G.; Knop-Gericke, A.; Schloegl, R. Phase Coexistence of Multiple Copper Oxides on AgCu Catalysts during Ethylene Epoxidation. *ACS Catal.* **2018**, *8*, 2286−2295.

(5) Greiner, M. T.; Jones, T. E.; Klyushin, A.; Knop-Gericke, A.; Schloegl, R. Ethylene Epoxidation at the Phase Transition of Copper Oxides. *J. Am. Chem. Soc.* **2017**, *139*, 11825−11832.

(6) Xu, H.; Zhu, L.; Nan, Y.; Xie, Y.; Cheng, D. Revisit the Role of Metal Dopants in Enhancing the Selectivity of Ag-Catalyzed Ethylene Epoxidation: Optimizing Oxophilicity of Reaction Site via Cocatalytic Mechanism. *ACS Catal.* **2021**, *11*, 3371−3383.

(7) Pu, T.; Tian, H.; Ford, M. E.; Rangarajan, S.; Wachs, I. E. Overview of Selective Oxidation of Ethylene to Ethylene Oxide by Ag Catalysts. *ACS Catal.* **2019**, *9*, 10727−10750.

(8) Serafin, J. G.; Liu, A. C.; Seyedmonir, S. R. Surface Science and the Silver-Catalyzed Epoxidation of Ethylene: An Industrial Perspective. *J. Mol. Catal. A* **1998**, *131*, 157−168.

(9) Lambert, R. M.; Williams, F. J.; Cropley, R. L.; Palermo, A. Heterogeneous Alkene Epoxidation: Past, Present and Future. *J. Mol. Catal. A* **2005**, *228*, 27−33.

(10) Christopher, P.; Linic, S. Engineering Selectivity in Heterogeneous Catalysis: Ag Nanowires as Selective Ethylene Epoxidation Catalysts. *J. Am. Chem. Soc.* **2008**, *130*, 11264−11265.

(11) Huš, M.; Hellman, A. Ethylene Epoxidation on Ag(100), Ag(110), and Ag(111): A Joint Ab Initio and Kinetic Monte Carlo Study and Comparison with Experiments. *ACS Catal.* **2019**, *9*, 1183−1196.

(12) Özbek, M. O.; van Santen, R. A. The Mechanism of Ethylene Epoxidation Catalysis. *Catal. Lett.* **2013**, *143*, 131−141.

(13) Kilty, P. A.; Sachtler, W. M. H. The Mechanism of the Selective Oxidation of Ethylene to Ethylene Oxide. *Catal. Rev.* **1974**, *10*, 1−16.

(14) Özbek, M. O.; Önal, I.; van Santen, R. A. Ethylene Epoxidation Catalyzed by Silver Oxide. *ChemCatChem* **2011**, *3*, 150−153.

(15) Özbek, M. O.; Onal, I.; van Santen, R. A. Why Silver Is the Unique Catalyst for Ethylene Epoxidation. *J. Catal.* **2011**, *284*, 230−235.

(16) Linic, S.; Barteau, M. A. Formation of a Stable Surface Oxametallacycle That Produces Ethylene Oxide. *J. Am. Chem. Soc.* **2002**, *124*, 310−317.

(17) Linic, S.; Piao, H.; Adib, K.; Barteau, M. A. Ethylene Epoxidation on Ag: Identification of the Crucial Surface Intermediate by Experimental and Theoretical Investigation of Its Electronic Structure. *Angew. Chem., Int. Ed.* **2004**, *43*, 2918−2921.

(18) Lukaski, A. C.; Barteau, M. A. Investigation of Ethylene Oxide on Clean and Oxygen-Covered Ag(110) Surfaces. *Catal. Lett.* **2009**, *128*, 9−17.

(19) Linic, S.; Barteau, M. A. Construction of a Reaction Coordinate and a Microkinetic Model for Ethylene Epoxidation on Silver from DFT Calculations and Surface Science Experiments. *J. Catal.* **2003**, *214*, 200−212.

(20) Medlin, J. W.; Barteau, M. A. The Formation of Epoxides from Reactions of Oxametallacycles on Ag(110): A Density Functional Theory Study. *J. Phys. Chem. B* **2001**, *105*, 10054−10061.

(21) Linic, S.; Barteau, M. A. Control of Ethylene Epoxidation Selectivity by Surface Oxametallacycles. *J. Am. Chem. Soc.* **2003**, *125*, 4034−4035.

(22) Böcklein, S.; Günther, S.; Reichelt, R.; Wyrwich, R.; Joas, M.; Hettstedt, C.; Ehrensperger, M.; Sicklinger, J.; Wintterlin, J. Detection and Quantification of Steady-State Ethylene Oxide Formation over an Ag(111) Single Crystal. *J. Catal.* **2013**, *299*, 129−136.

(23) Campbell, C. The Selective Epoxidation of Ethylene Catalyzed by Ag(111) − a Comparison with Ag(110). *J. Catal.* **1985**, *94*, 436−444.

(24) Rocha, T. C. R.; Oestereich, A.; Demidov, D. V.; Hävecker, M.; Zafeiratos, S.; Weinberg, G.; Bukhtiyarov, V. I.; Knop-Gericke, A.; Schlögl, R. The Silver−Oxygen System in Catalysis: New Insights by near Ambient Pressure X-Ray Photoelectron Spectroscopy. *Phys. Chem. Chem. Phys.* **2012**, *14*, 4554−4564.

(25) Jones, T. E.; Rocha, T. C. R.; Knop-Gericke, A.; Stampfl, C.; Schloegl, R.; Piccinin, S. Thermodynamic and Spectroscopic Properties of Oxygen on Silver under an Oxygen Atmosphere. *Phys. Chem. Chem. Phys.* **2015**, *17*, 9288−9312.

(26) Böcklein, S.; Gunther, S.; Wintterlin, J. High-Pressure Scanning Tunneling Microscopy of a Silver Surface during Catalytic Formation of Ethylene Oxide. *Angew. Chem., Int. Ed.* **2013**, *52*, 5518−5521.

(27) Günther, S.; Boecklein, S.; Wintterlin, J.; Nino, M. A.; Mentes, T. O.; Locatelli, A. Locating Catalytically Active Oxygen on Ag(111)-A Spectromicroscopy Study. *ChemCatChem* **2013**, *5*, 3342−3350.

(28) Carbonio, E. A.; Rocha, T. C. R.; Klyushin, A. Y.; Pis, I.; Magnano, E.; Nappini, S.; Piccinin, S.; Knop-Gericke, A.; Schloegl, R.; Jones, T. E. Are Multiple Oxygen Species Selective in Ethylene Epoxidation on Silver? *Chem. Sci.* **2018**, *9*, 990−998.

(29) Jones, T. E.; Wyrwich, R.; Boecklein, S.; Carbonio, E. A.; Greiner, M. T.; Klyushin, A. Y.; Moritz, W.; Locatelli, A.; Mentes, T. O.; Nino, M. A.; Knop-Gericke, A.; Schloegl, R.; Guenther, S.; Wintterlin, J.; Piccinin, S. The Selective Species in Ethylene Epoxidation on Silver. *ACS Catal.* **2018**, *8*, 3844−3852.

(30) Wyrwich, R.; Jones, T. E.; Günther, S.; Moritz, W.; Ehrensperger, M.; Böcklein, S.; Zeller, P.; Lünser, A.; Locatelli, A.; Menteş, T. O.; Niño, M. Á.; Knop-Gericke, A.; Schlögl, R.; Piccinin, S.; Wintterlin, J. LEED- I (V) Structure Analysis of the $(7 \times \sqrt{3})$Rect SO$_4$ Phase on Ag(111): Precursor to the Active Species of the Ag-Catalyzed Ethylene Epoxidation. *J. Phys. Chem. C* **2018**, *122*, 26998−27004.

(31) Kenge, N.; Pitale, S.; Joshi, K. The Nature of Electrophilic Oxygen: Insights from Periodic Density Functional Theory Investigations. *Surf. Sci.* **2019**, *679*, 188−195.

(32) Michaelides, A.; Reuter, K.; Scheffler, M. When Seeing Is Not Believing: Oxygen on Ag(111), a Simple Adsorption System? *J. Vac. Sci. Technol. A* **2005**, *23*, 1487−1497.

(33) Martin, N. M.; Klacar, S.; Gronbeck, H.; Knudsen, J.; Schnadt, J.; Blomberg, S.; Gustafson, J.; Lundgren, E. High-Coverage Oxygen-Induced Surface Structures on Ag(111). *J. Phys. Chem. C* **2014**, *118*, 15324−15331.

(34) van den Reijen, J. E.; Kanungo, S.; Welling, T. A. J.; Versluijs-Helder, M.; Nijhuis, T. A.; de Jong, K. P.; de Jongh, P. E. Preparation and Particle Size Effects of Ag/α-Al$_2$O$_3$ Catalysts for Ethylene Epoxidation. *J. Catal.* **2017**, *356*, 65−74.

(35) van Hoof, A. J. F.; Filot, I. A. W.; Friedrich, H.; Hensen, E. J. M. Reversible Restructuring of Silver Particles during Ethylene Epoxidation. *ACS Catal.* **2018**, *8*, 11794−11800.

(36) Derouin, J.; Farber, R. G.; Heslop, S. L.; Killelea, D. R. Formation of Surface Oxides and Ag$_2$O Thin Films with Atomic Oxygen on Ag(111). *Surf. Sci.* **2015**, *641*, L1−L4.

(37) Derouin, J.; Farber, R. G.; Turano, M. E.; Iski, E. V.; Killelea, D. R. Thermally Selective Formation of Subsurface Oxygen in Ag(111) and Consequent Surface Structure. *ACS Catal.* **2016**, *6*, 4640−4646.

(38) Turano, M. E.; Farber, R. G.; Oskorep, E. C. N.; Rosenberg, R. A.; Killelea, D. R. Characterization of Oxygenaceous Species Formed by Exposure of Ag(111) to Atomic Oxygen. *J. Phys. Chem. C* **2020**, *124*, 1382−1389.

(39) Shang, C.; Liu, Z.-P. Stochastic Surface Walking Method for Structure Prediction and Pathway Searching. *J. Chem. Theory Comput.* **2013**, *9*, 1838−1845.

(40) Zhang, X.-J.; Shang, C.; Liu, Z.-P. From Atoms to Fullerene: Stochastic Surface Walking Solution for Automated Structure Prediction of Complex Material. *J. Chem. Theory Comput.* **2013**, *9*, 3252−3260.

(41) Huang, S.-D.; Shang, C.; Zhang, X.-J.; Liu, Z.-P. Material Discovery by Combining Stochastic Surface Walking Global Optimization with a Neural Network. *Chem. Sci.* **2017**, *8*, 6327−6337.

(42) Huang, S.-D.; Shang, C.; Kang, P.-L.; Liu, Z.-P. Atomic Structure of Boron Resolved Using Machine Learning and Global Sampling. *Chem. Sci.* **2018**, *9*, 8644−8655.

(43) Li, Y.-F.; Zhu, S.-C.; Liu, Z.-P. Reaction Network of Layer-to-Tunnel Transition of MnO$_2$. *J. Am. Chem. Soc.* **2016**, *138*, 5371−5379.

(44) Xie, Y.-P.; Zhang, X.-J.; Liu, Z.-P. Graphite to Diamond: Origin for Kinetics Selectivity. *J. Am. Chem. Soc.* **2017**, *139*, 2545−2548.

(45) Kang, P.-L.; Shang, C.; Liu, Z.-P. Glucose to 5-Hydroxymethylfurfural: Origin of Site-Selectivity Resolved by Machine Learning Based Reaction Sampling. *J. Am. Chem. Soc.* **2019**, *141*, 20525−20536.

(46) Zhang, X.-J.; Shang, C.; Liu, Z.-P. Double-Ended Surface Walking Method for Pathway Building and Transition State Location of Complex Reactions. *J. Chem. Theory Comput.* **2013**, *9*, 5745−5753.

(47) Shang, C.; Liu, Z.-P. Constrained Broyden Dimer Method with Bias Potential for Exploring Potential Energy Surface of Multistep Reaction Process. *J. Chem. Theory Comput.* **2012**, *8*, 2215−2222.

(48) Kresse, G.; Furthmüller, J. Efficient Iterative Schemes for *Ab Initio* Total-Energy Calculations Using a Plane-Wave Basis Set. *Phys. Rev. B* **1996**, *54*, No. 11169.

(49) Kresse, G.; Joubert, D. From Ultrasoft Pseudopotentials to the Projector Augmented-Wave Method. *Phys. Rev. B* **1999**, *59*, No. 1758.

(50) Perdew, J. P.; Burke, K.; Ernzerhof, M. Generalized Gradient Approximation Made Simple. *Phys. Rev. Lett.* **1996**, *77*, No. 3865.

(51) Lide, R. D. *CRC Handbook of Chemistry and Physics*, 95th ed.; CRC Press: New York, 2015.

(52) Tang, Q.-L.; Hong, Q.-J.; Liu, Z.-P. CO$_2$ Fixation into Methanol at Cu/ZrO$_2$ Interface from First Principles Kinetic Monte Carlo. *J. Catal.* **2009**, *263*, 114−122.

(53) Özbek, M. O.; Onal, I.; van Santen, R. A. Effect of Surface and Oxygen Coverage on Ethylene Epoxidation. *Top. Catal.* **2012**, *55*, 710−717.

(54) Stegelmann, C.; Stoltze, P. Microkinetic Analysis of Transient Ethylene Oxidation Experiments on Silver. *J. Catal.* **2004**, *226*, 129−137.

(55) Li, X.-T.; Chen, L.; Wei, G.-F.; Shang, C.; Liu, Z.-P. Sharp Increase in Catalytic Selectivity in Acetylene Semihydrogenation on Pd Achieved by a Machine Learning Simulation-Guided Experiment. *ACS Catal.* **2020**, *10*, 9694−9705.

(56) Schmid, M.; Reicho, A.; Stierle, A.; Costina, I.; Klikovits, J.; Kostelnik, P.; Dubay, O.; Kresse, G.; Gustafson, J.; Lundgren, E.; Andersen, J. N.; Dosch, H.; Varga, P. Structure of Ag(111)-p(4 × 4)-O: No Silver Oxide. *Phys. Rev. Lett.* **2006**, *96*, No. 146102.

(57) Schnadt, J.; Michaelides, A.; Knudsen, J.; Vang, R. T.; Reuter, K.; Laegsgaard, E.; Scheffler, M.; Besenbacher, F. Revisiting the Structure of the p(4 × 4) Surface Oxide on Ag(111). *Phys. Rev. Lett.* **2006**, *96*, No. 146101.

(58) Jones, T. E.; Wyrwich, R.; Boecklein, S.; Rocha, T. C. R.; Carbonio, E. A.; Knop-Gericke, A.; Schloegl, R.; Guenther, S.; Wintterlin, J.; Piccinin, S. Oxidation of Ethylene on Oxygen Reconstructed Silver Surfaces. *J. Phys. Chem. C* **2016**, *120*, 28630−28638.

(59) Tarrat, N.; Rapacioli, M.; Cuny, J.; Morillo, J.; Heully, J.-L.; Spiegelman, F. Global Optimization of Neutral and Charged 20- and 55-Atom Silver and Gold Clusters at the DFTB Level. *Comput. Theor. Chem.* **2017**, *1107*, 102−114.

(60) Reinhard, D.; Hall, B. D.; Ugarte, D.; Monot, R. Size-Independent Fcc-to-Icosahedral Structural Transition in Unsupported Silver Clusters: An Electron Diffraction Study of Clusters Produced by Inert-Gas Aggregation. *Phys. Rev. B* **1997**, *55*, No. 7868.

(61) Rapacioli, M.; Spiegelman, F.; Tarrat, N. Evidencing the Relationship between Isomer Spectra and Melting: The 20- and 55-Atom Silver and Gold Cluster Cases. *Phys. Chem. Chem. Phys.* **2019**, *21*, 24857−24866.

(62) Torres, D.; Lopez, N.; Illas, F.; Lambert, R. M. Why Copper Is Intrinsically More Selective than Silver in Alkene Epoxidation: Ethylene Oxidation on Cu(111) versus Ag(111). *J. Am. Chem. Soc.* **2005**, *127*, 10774−10775.

(63) Torres, D.; Illas, F. On the Performance of Au(111) for Ethylene Epoxidation: A Density Functional Study. *J. Phys. Chem. B* **2006**, *110*, 13310−13313.

(64) Bader, R. A Quantum-Theory of Molecular-Structure and Its Applications. *Chem. Rev.* **1991**, *91*, 893−928.

(65) Kokalj, A.; Gava, P.; Degironcoli, S.; Baroni, S. What Determines the Catalyst's Selectivity in the Ethylene Epoxidation Reaction. *J. Catal.* **2008**, *254*, 304−309.

(66) Waugh, K. C.; Hague, M. The Detailed Kinetics and Mechanism of Ethylene Epoxidation on an Oxidised Ag/Alpha-Al$_2$O$_3$ Catalyst. *Catal. Today* **2010**, *157*, 44−48.

(67) Couves, J.; Atkins, M.; Hague, M.; Sakakini, B. H.; Waugh, K. C. The Activity and Selectivity of Oxygen Atoms Adsorbed on a Ag/Alpha-Al$_2$O$_3$ Catalyst in Ethene Epoxidation. *Catal. Lett.* **2005**, *99*, 45−53.

(68) Bukhtiyarov, V.; Prosvirin, I.; Kvon, R. Study of Reactivity of Oxygen States Adsorbed at a Silver Surface Towards C$_2$H$_4$ by XPS, TPD and TPR. *Surf. Sci.* **1994**, *320*, L47−L50.

(69) Jingfa, D.; Jun, Y.; Shi, Z.; Xiaohong, Y. Promoting Effects of Re and Cs on Silver Catalyst in Ethylene Epoxidation. *J. Catal.* **1992**, *138*, 395−399.

(70) Rebsdat, S.; Mayer, D. Ethylene Oxide. In *Ullmann's Encyclopedia of Industrial Chemistry*; American Cancer Society, 2001.